hydrology

MDPI

Article

Quantifying the Role of Urban Development and Rainfall Shifts in Dynamic Hydrological Extremes

Wati Asriningsih Pranoto [1,*], Rijal Muhammad Fikri [1], Doddi Yudianto [2], Steven Reinaldo Rusli [2] and Obaja Triputera Wijaya [2]

[1] Civil Engineering, Tarumanagara University, Jakarta 11440, Indonesia; rijal.328241004@stu.untar.ac.id
[2] Department of Civil Engineering, Parahyangan Catholic University, Bandung 40141, Indonesia; doddi_yd@unpar.ac.id (D.Y.); steven.reinaldo@unpar.ac.id (S.R.R.); obaja.wijaya@unpar.ac.id (O.T.W.)
* Correspondence: watip@ft.untar.ac.id

Abstract

Urbanization, together with shifts in rainfall patterns, has become an increasingly important driver of hydrological extremes in many rapidly developing tropical regions. In the Cimanceuri River Basin, Tangerang Regency, Indonesia, these processes have intensified over the last decade, raising concerns regarding flood risk. This study examines the combined influence of urban expansion and rainfall variability on flood dynamics over 2013–2025. Multi temporal land use classification based on Landsat imagery indicates a pronounced growth of impervious surfaces, primarily driven by rapid urban development and the conversion of agricultural land. To assess the hydrological consequences of these changes, rainfall–runoff processes and flood inundation were simulated using the Soil Conservation Service Curve Number (SCS–CN) method within a coupled HEC-HMS and HEC-RAS 2D modelling framework. Simulations were performed for multiple temporal conditions and design rainfall scenarios. Model calibration relied on observed flood events recorded in March 2025 in the Mustika Residential Area, Tangerang. The results suggest that urbanization has contributed to measurable increases in both peak discharge and inundation extent. Between 2013 and 2025, impervious surface coverage expanded by approximately 67%, accompanied by a rise in the composite Curve Number from 85.86 to 86.63 and an estimated 5.2% increase in flood extent. Also, the design rainfall increased from 85.01 to 90.95 with an average increase of 7.34%. Comparison between simulated inundation patterns and aerial imagery shows satisfactory agreement, with an average deviation of less than 10%, indicating acceptable model performance. Hydrologic analyses generated two discharge scenarios, consisting of event-based flow from the 5 March 2025 rainfall data and return-period flows derived from design rainfall under different rainfall-shift periods. The rainfall-shift analysis quantified changes in design rainfall and corresponding discharge using progressively updated rainfall records. Together, the results emphasize the combined effects of urban expansion and shifting rainfall patterns on flood dynamics, underscoring the need for adaptive land-use planning and climate-responsive water management in rapidly urbanizing catchments.

Keywords: urbanization; flood; hydrological extremes; land use change; HEC-RAS; HEC-HMS; Cimanceuri River

Check for updates

Academic Editors: Fabio Russo and Andrea Petroselli

Received: 13 March 2026
Revised: 24 April 2026
Accepted: 25 April 2026
Published: 30 April 2026

Copyright: © 2026 by the authors. Licensee MDPI, Basel, Switzerland. This article is an open access article distributed under the terms and conditions of the Creative Commons Attribution (CC BY) license.

1. Introduction

Indonesia represents a highly relevant case study due to its rapid urbanization, high rainfall intensity, and frequent flood occurrences in tropical environments. The Cimanceuri

River Basin reflects typical conditions of developing urban catchments, where land-use conversion and climate variability interact to intensify flood risk. Previous studies have demonstrated that urban expansion significantly increases surface runoff and flood susceptibility through the growth of impervious surfaces, which reduce infiltration capacity and accelerate peak discharge [1,2]. At the same time, changes in rainfall patterns driven by climate variability further amplify hydrological extremes and flood hazards, particularly when interacting with urban land-use changes [3].

Despite numerous studies on flood hazards, limited research has quantitatively integrated multi-temporal land-use change and rainfall variability within a unified modelling framework. Existing studies often highlight the individual impacts of urbanization or climate variability, yet the complex interactions between these drivers remain insufficiently quantified, particularly in rapidly developing regions [2,3].

To provide a broader context, disasters can be defined as a disruption to social order and environmental conditions due to a hazard, which results in physical, economic, and social damage [4]. Disasters can be categorized in various ways, including floods, landslides, earthquakes, forest fires, and droughts. There are several characteristics and levels of risk of disasters, resulting in increased damage to the natural environment [5]. Thus, to minimize losses to society due to disasters, mitigation is needed as an effort to minimize and prevent the high risk of loss of life and property [6].

From the various types of disasters, floods remain one of the most destructive hydrological disasters worldwide, especially in tropical regions experiencing rapid land cover transformation and climate variability, and their occurrence is becoming more frequent due to global warming and climate change [7–9]. Floods are a natural disaster that continually threatens lives and property [10]. Over the past 30 years, floods have become the world's most devastating natural disaster, affecting nearly 80 million people annually [11,12]. At the global scale, climate change has significantly altered the hydrological cycle by intensifying precipitation extremes, modifying rainfall distribution, and increasing the frequency of short-duration high-intensity storms, all of which contribute to rising flood risk. Furthermore, warming atmospheric conditions increase moisture-holding capacity, leading to more intense rainfall events, particularly in tropical and monsoon regions where flood hazards are already prevalent [13]. The increasing frequency and intensity of floods have been closely linked to two dominant factors, urban development and shifts in rainfall patterns [14]. Climate change is also considered to be the leading causal factor of flood-inducing rainstorms [15]. However, these two drivers are often treated separately, whereas their interaction can amplify flood responses and create more complex and localized hydrological extremes.

Urbanization, particularly the expansion of impervious surfaces such as roads, buildings, and pavement, significantly reduces infiltration and natural storage while accelerating surface runoff and peak discharges [16]. This phenomenon has become increasingly significant as urban areas continue to expand rapidly, altering natural hydrological processes and increasing flood susceptibility. In developing countries such as Indonesia, urban growth is often characterized by rapid and unplanned land-use conversion, accompanied by limited drainage capacity, which further exacerbates flood risks. Rapid urban expansion increases impervious surface areas, reducing infiltration capacity and accelerating surface runoff, thereby intensifying flood hazards and peak discharge [17]. In addition, inadequate urban drainage systems and uncontrolled land development in many cities contribute to the increasing frequency and severity of urban flooding [18]. These processes, combined with increasing rainfall variability, have been widely recognized as key drivers of urban flood risk. Consequently, the combined effects of urbanization and rainfall changes have received growing attention in recent hydrological and flood risk studies [17].

For instance, studies in Kuala Lumpur and other Asian megacities found that hourly rainfall extremes increased by up to 35% due to urban-induced convection [19]. Similar trends have been observed in European suburban areas, where warm climates and urban sprawl jointly intensified localized rainfall [20]. Previous studies further demonstrate that urbanization can disproportionately intensify short-duration rainfall extremes, with stronger effects observed at the hourly scale compared to daily rainfall, thereby amplifying flood-generating processes in urban catchments [21]. In addition, integrated hydrological analyses have shown that the interaction between urban expansion and extreme rainfall not only increases runoff generation but also alters infiltration dynamics and basin response, highlighting the need for models that explicitly capture these coupled processes [22]. Global evidence shows that extreme short-duration rainfall is intensifying due to climate change, increasing the likelihood of flash floods and emphasizing the need for improved understanding and adaptation strategies [23].

Floods in Indonesia exhibit distinct characteristics influenced by its tropical monsoon climate, complex archipelagic setting, and diverse topography [24]. Indonesia experiences a pronounced seasonal rainfall pattern associated with the monsoon system, where the wet season is typically characterized by intense and persistent precipitation that frequently leads to flooding. Extreme rainfall events are a primary driver of flood occurrence, often linked to large-scale atmospheric variability such as ENSO, Madden–Julian Oscillation (MJO), and cross-equatorial moisture transport, as well as mesoscale convective systems that enhance precipitation intensity and duration [24,25]. These processes can trigger different types of flooding, including riverine floods, flash floods, and coastal flooding, depending on local hydrological and geographical conditions. In rapidly urbanizing regions, such as parts of Java, flood risk is further exacerbated by land-use change, increasing impervious surfaces, and reduced infiltration capacity, which contribute to higher runoff and flood frequency [26]. The interaction between extreme rainfall, land-use change, and regional hydro-meteorological processes highlights the complexity of flood dynamics in Indonesia and underscores the need for integrated hydrological and hydraulic modelling approaches.

Despite growing recognition of urbanization and rainfall shifts as dual stressors in flood risk amplification, quantitative studies integrating both aspects within a dynamic, multi-temporal hydrological–hydrodynamic framework remain limited—particularly in the context of tropical developing countries. Existing studies in Indonesia have predominantly assessed flood risk using static land use datasets or without explicit rainfall frequency analysis, leading to incomplete representation of temporal dynamics.

Hydrological and hydraulic models are widely used to simulate rainfall–runoff processes and flood inundation dynamics in watershed systems. The HEC-HMS model has been extensively applied for rainfall–runoff simulation due to its simplicity and capability to represent watershed hydrological processes, including loss, transformation, and routing components [27]. For floodplain analysis, hydraulic models such as HEC-RAS are commonly used to simulate water flow, inundation depth, and velocity under various boundary conditions [28]. The integration of HEC-HMS and HEC-RAS within a GIS environment has become a widely adopted approach for flood hazard assessment, enabling the coupling of hydrological processes with hydraulic floodplain dynamics and supporting the generation of flood hazard maps under different return period scenarios [29].

For example, studies applying HEC-HMS and HEC-RAS in Indonesian river basins and urban watersheds generally focus on single-event simulations or fixed land-use conditions, which are effective for reproducing observed floods but do not capture the cumulative impact of urban expansion over time [30,31]. Similarly, flood hazard assessments based on land-use change often evaluate spatial impacts under predefined scenarios, yet they lack integration with evolving rainfall characteristics, limiting their ability to represent cou-

pled hydro-climatic dynamics [32]. This limitation makes it difficult to capture how flood risk evolves over time, especially in rapidly urbanizing basins where both land surface characteristics and rainfall regimes are changing simultaneously.

To address these limitations, this study develops an integrated multi-temporal hydrologic–hydrodynamic framework that explicitly links land-use change and rainfall variability to flood response. The integration of hydrological and hydraulic modelling approaches has been widely recognized as an effective method for simulating flood processes and improving the understanding of urban flood dynamics [33]. The approach combines multi-temporal land-use analysis (2013–2025), rainfall-shift analysis, and event-based hydrodynamic simulation to capture the evolving nature of hydrological extremes in a rapidly urbanizing tropical basin.

Unlike previous studies that rely on static land-use conditions or single-model approaches, integrated and multi-modelling frameworks have been increasingly applied to better capture uncertainties and improve the representation of flood characteristics under changing environmental conditions [34]. By translating these interactions into spatially distributed inundation patterns, the study provides a more comprehensive representation of how flood risk develops over time and offers improved insight for adaptive flood management and urban planning.

2. Materials and Methods

2.1. Study Area

This study was conducted in the Cimanceuri Watershed, located in Tangerang Regency, Banten Province, Indonesia. The Cimanceuri River, located within the administrative boundaries of Tangerang Regency, extends approximately 86.97 km and exhibits a channel width ranging from 10 to 20 m. In addition to the main river flow originating from upstream catchments, the Cimanceuri also functions as a confluence point for several tributaries and urban drainage channels, which collectively contribute to its hydrological complexity and flood potential. The catchment area represents a rapidly urbanizing watershed where agricultural and vegetated lands have gradually been converted into residential and industrial zones over the past decade, significant transformations in land cover patterns were observed, primarily driven by rapid urban development. These changes are mainly driven by rapid urbanization in the study area. This transformation has significantly influenced the watershed's hydrological response, particularly in terms of infiltration capacity and surface runoff. The Cimanceuri River flows through mixed land use areas characterized by low relief terrain and a tropical monsoon climate, where intense rainfall frequently leads to localized flooding. Cimanceuri River flows through mixed land use areas characterized by low relief terrain and a tropical monsoon climate, where intense rainfall frequently leads to localized flooding during the wet season from November to April. Historically, this area has experienced recurrent flood events, particularly during peak rainy seasons, with several inundation incidents reported in residential areas along the river due to limited drainage capacity and rapid land-use change. These recurring flood events highlight the vulnerability of the watershed and support its selection as a relevant study area for flood analysis.

This study specifically focuses on a selected sub-basin of the Cimanceuri tributary (Figure 1), which serves as a representative area to analyze the hydrological response to land-use changes and rainfall variability. Although relatively small in size, the selected sub-basin exhibits key characteristics of the broader watershed, including rapid land-use conversion, high runoff sensitivity, and frequent flood occurrences. These features make it a suitable representative unit for capturing the dominant hydrological processes influenced by urbanization and rainfall variability. Historically, the study area has experienced fre-

quent flood events, including major flooding in 2007, with recurrent inundations reported during the period 2005–2019. More recent events include severe flooding on 17 March 2020 and 19–20 May 2020, the latter being one of the most significant events since 2007, inundating hundreds of houses with water depths reaching up to 1.5 m. Additional flood occurrences were recorded in February and August 2021, and more recently in April 2026 due to high-intensity rainfall. The sub-basin was chosen based on its sensitivity to runoff generation, rapid land conversion, and proximity to urban development zones that have experienced recurrent flooding. By narrowing the analysis to this sub-catchment, the study aims to provide a more detailed understanding of localized hydrological dynamics within the broader Cimanceuri Watershed system. Additionally, aerial imagery of the March 2025 flood event in the Mustika Residential Area was utilized for model calibration (Figure 1). The aerial photographs provided by local authorities captured the actual flood extent and depth distribution, which were compared against the simulated inundation maps to evaluate model accuracy and reliability.

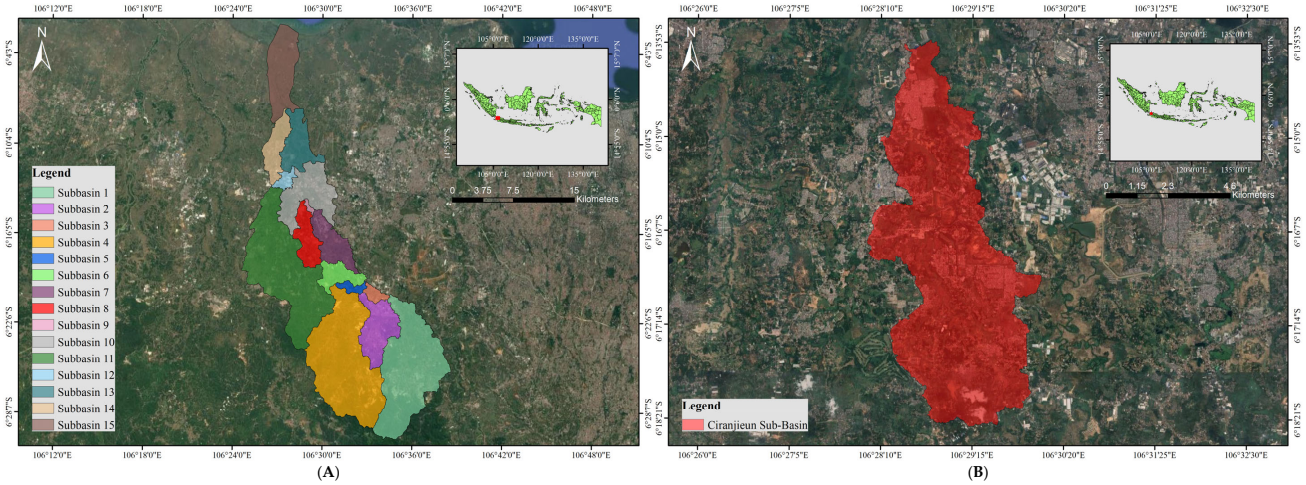


Figure 1. Study area: (**A**) Cimanceuri sub-basins, with Sub-basin 8 indicating the selected detailed study area; (**B**) detailed map of Sub-basin 8 or Ciranjieun Sub-basin, which is the focus area of this study. In the inset map, the green highlighted area represents Indonesia, while the red dot indicates the study location.

2.2. Methodology

This study adopts an integrated hydrologic–hydraulic modeling framework consisting of five main stages: event-based hydrological analysis, two-dimensional (2D) hydraulic simulation of the observed event, two-dimension model calibration, rainfall-shift analysis, and scenario-based 2D flood simulations incorporating rainfall variability and land-use change. The overall workflow of the study is illustrated in Figure 2.

Two-dimensional (2D) hydrodynamic models are increasingly used to simulate these complex interactions, offering improved accuracy in predicting inundation extents and velocities compared to traditional one-dimensional (1D) models [35]. In Indonesia, several studies have applied hydrodynamic modeling for flood risk assessment, including in urban watersheds [36,37]. Flood risk has intensified due to rapid urbanization, land use and land cover changes, and the conversion of green open spaces into built-up areas, which collectively increase surface runoff and river discharge [38]. In addition, land use and land cover changes induced by urbanization not only impact local weather and climate patterns, but also modify urban hydrologic responses and hydraulics, thus making urban areas more prone to flash floods [39]. Land use change from 2014 to 2024 was mapped using satellite imagery and spatial analysis, revealing a significant increase in impervious surfaces due to rapid urban expansion. Concurrently, rainfall data analysis indicated a trend toward more

intense, shorter-duration events, exemplified by the flood on 5 March 2025, which caused widespread inundation in the Mustika Residential Area.

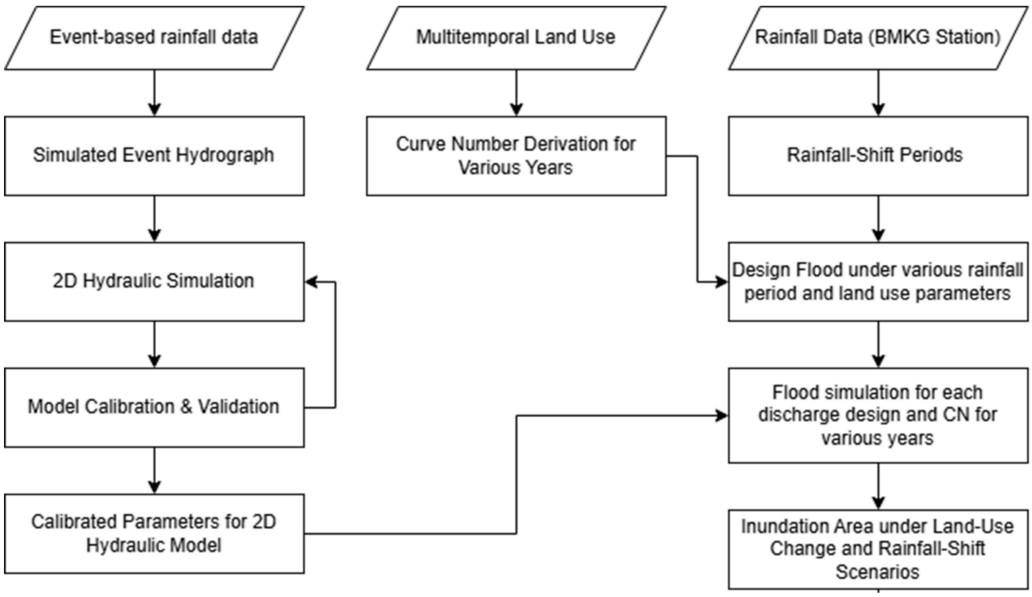


Figure 2. Research methodology framework.

To carry out the analysis, two modeling tools developed by the U.S. Army Corps of Engineers were used: the Hydrologic Engineering Center–Hydrologic Modeling System (HEC-HMS) and the Hydrologic Engineering Center–River Analysis System (HEC-RAS). HEC-HMS is designed to simulate the complete hydrologic processes of dendritic watershed systems, including rainfall losses, unit hydrograph transformation, and hydrologic routing [32]. Meanwhile, HEC-RAS can perform one- and two-dimensional hydraulic calculations for natural and engineered river systems, floodplains, and related hydraulic structures [35]. In this study, only the 2D hydraulic module of HEC-RAS was utilized to capture spatial flood dynamics across the floodplain.

The first stage focused on event-based hydrological modeling using observed rainfall data from the 5 March 2025 flood event. Rainfall–runoff transformation was carried out in HEC-HMS to generate the event-based discharge hydrograph. Multi-temporal land-use data were processed and classified to derive Curve Number (CN) values using the Soil Conservation Service Curve Number (SCS-CN) method. The CN values were obtained by overlaying land-use and soil-type maps to represent spatial variations in infiltration capacity and runoff potential. These parameters were incorporated into HEC-HMS to simulate basin response during the event.

The resulting event-based discharge hydrograph was then applied as the upstream boundary condition in the 2D hydraulic model developed in HEC-RAS. Subsequently, the 2D hydraulic model was calibrated by adjusting Manning's roughness coefficient (n) to achieve agreement between simulated and observed inundation extents in the Mustika Residential Area. Calibration was performed through comparison of simulated flood area and water depth with independent flood observation data to ensure model robustness and reliability.

Flood inundation modelling was performed through calibrated hydrological and hydraulic simulations using both event-based and return-period rainfall scenarios. The 5 March 2025 storm was simulated in HEC-HMS by applying the event hyetograph together with year-specific CN maps derived from Landsat 7 land-use classifications (2013, 2017, 2021, 2025). Resulting runoff hydrographs were used as upstream boundary inputs in HEC-

RAS 2D, configured with mesh resolutions of 5–20 m and computational time steps of 1–5 s in accordance with DEM accuracy and Courant stability requirements. Each simulation produced spatial outputs of maximum depth, inundation extent, and flood duration.

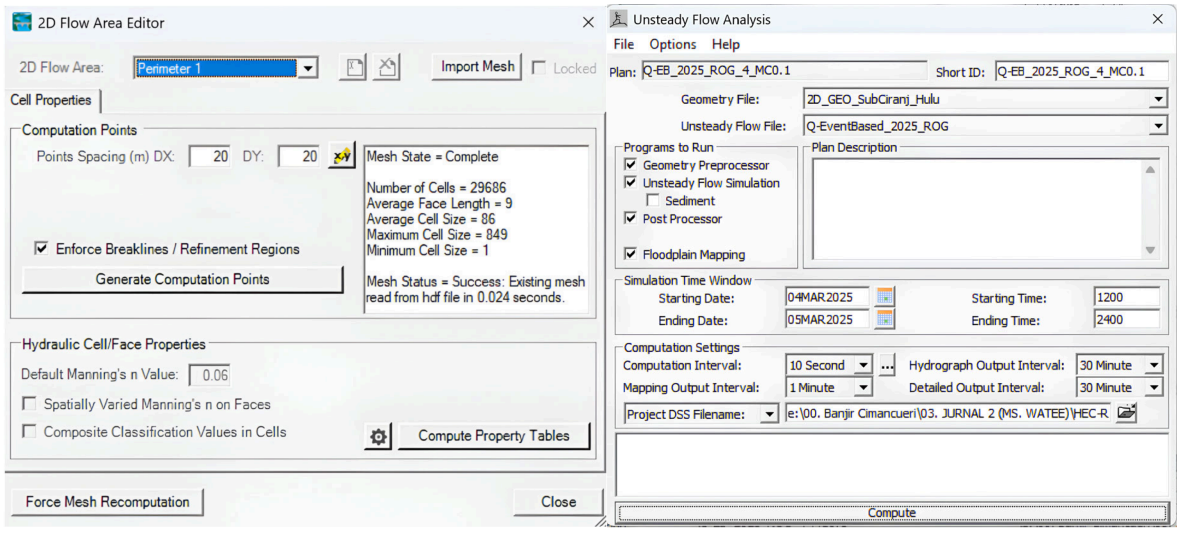
All hydraulic results were post-processed in a GIS environment to generate standardized flood maps and spatial statistics, enabling comparison of inundation extent, depth variation, and exposure of assets across land-use scenarios. Sensitivity analyses on Manning's n and CN values were conducted to quantify model uncertainty and support the robustness of flood risk assessments.

To capture broader flood behaviour beyond the observed event, a rainfall-shift analysis was carried out using extended rainfall records from the Budiarto BMKG Station. Frequency analysis in Hydrognomon provided updated return-period rainfall estimates, which were transformed into design discharge hydrographs using the calibrated HEC-HMS model. These discharge design hydrographs incorporating annual land-use conditions and CN values were subsequently used in hydraulic simulations to evaluate flood responses under multiple rainfall shift and land use configurations.

Frequency analysis and consistency testing were then performed to derive updated design rainfall that reflects temporal shifts in rainfall characteristics.

The hydraulic model setup was conducted by defining the 2D flow area and generating a computational mesh with a spatial resolution of 20 × 20 m, producing 2966 cells and 8649 faces. This mesh resolution was selected to maintain a balance between spatial detail and computational efficiency in representing urban floodplain dynamics.

For the unsteady flow simulation, the computation time step was set to 10 s, with a mapping output interval of 1 min and a hydrograph output interval of 30 min. The simulation period covered 4–5 March 2025, corresponding to the observed flood event. These parameter settings ensured numerical stability while providing sufficient temporal resolution to capture variations in discharge and flood depth. The configuration of the 2D model, including flow area definition and unsteady flow parameters, is shown in Figure 3.



(**A**) (**B**)

Figure 3. HEC-RAS 2D model setup: (**A**) 2D flow area and mesh configuration, (**B**) unsteady flow simulation parameters.

The hydraulic model was subsequently calibrated by adjusting Manning's roughness coefficient (n) to achieve agreement between simulated and observed inundation extent and water depth in the Mustika Residential Area. Calibration was performed through

comparison of simulated flood extent and water depth with independent flood observation data derived from aerial imagery.

Following calibration, rainfall-shift analysis was conducted using long-term rainfall records from the Budiarto Meteorological BMKG Station. Prior to analysis, rainfall data were pre-processed and verified using Hydrognomon to ensure data quality and consistency. Frequency analysis and consistency testing were then performed to derive updated design rainfall that reflects temporal shifts in rainfall characteristics.

The analysis was conducted using a statistical distribution approach (e.g., Gave Max Likelihood Moments distribution) implemented in Hydrognomon to estimate design rainfall for selected return periods. The return periods of 2, 5, 10, and 25 years were selected as they represent commonly used design standards in hydrological studies and flood risk assessment, capturing both frequent and moderate flood events.

All spatial datasets were standardized to a common coordinate system and grid resolution to ensure spatial consistency. Data preprocessing, hydrological computation, and hydraulic simulations were performed using QGIS (version 3.34) for spatial processing, HEC-HMS (version 4.13) for rainfall–runoff modelling, Hydrognomon 4 for rainfall frequency analysis, and HEC-RAS (version 6.6) for 2D flood inundation simulation.

Finally, the calibrated 2D hydraulic model was used to simulate flood inundation under various rainfall-shift scenarios combined with land-use conditions from 2014 to 2024. This enabled assessment of how urban expansion and changing rainfall patterns influence flood discharge, flow dynamics, and inundation extent across the Cimanceuri watershed. Comparative analysis among scenarios was conducted to quantify the individual and combined effects of land-use transformation and rainfall variability on flood behaviour.

Model Performance Evaluation

Model performance during calibration was evaluated using the Root Mean Square Error (RMSE) and Nash–Sutcliffe Efficiency (NSE), which are widely applied in hydrological modeling to assess agreement between observed and simulated data [40].

RMSE measures the average magnitude of simulation error, while NSE evaluates the model's predictive capability relative to the mean of observed values. A lower RMSE indicates better model accuracy.

$$\mathrm{RMSE} = \sqrt{\frac{1}{n}\sum_{i=1}^{n}\left(Q_{obs,i} - Q_{sim,i}\right)^2}$$

where $Q_{obs,i}$ is the observed value, $Q_{sim,i}$ is the simulated value, and n is the number of observations.

In addition, the Nash–Sutcliffe Efficiency (NSE) was applied to evaluate the predictive performance of the model relative to the mean of observed data. NSE values range from $-\infty$ to 1, where a value of 1 indicates perfect agreement, while values closer to 0 or negative indicate poor model performance.

$$\mathrm{NSE} = 1 - \frac{\sum_{i=1}^{n}\left(Q_{obs,i} - Q_{sim,i}\right)^2}{\sum_{i=1}^{n}\left(Q_{obs,i} - \overline{Q_{obs}}\right)^2}$$

where $\overline{Q_{obs}}$ is the mean of observed values. Both RMSE and NSE were used as complementary indicators during the calibration process to ensure that the model is able to reproduce observed flood characteristics with acceptable accuracy. These metrics provide a quantitative basis for evaluating model performance prior to its application in scenario-based simulations.

2.3. Data Collection

2.3.1. Meteorological Data

Rainfall data were grouped into two types: event-based data and long-term historical data. The 5 March 2025 flood event rainfall was obtained from the Automatic Rainfall Recorder (ARR), which has a measurement accuracy of approximately ±0.2 mm, consistent with the standard performance of tipping-bucket rain gauges commonly used in hydrological monitoring, operated by the Tangerang Regency Public Works and Water Resources Agency. The data were used to develop the observed hydrograph for model calibration in HEC-HMS and HEC-RAS 2D. The temporal distribution of the event-based rainfall used for calibration is shown in Figure 4, which presents the hourly rainfall intensity recorded by the Balaraja ARR on 4–5 March 2025.

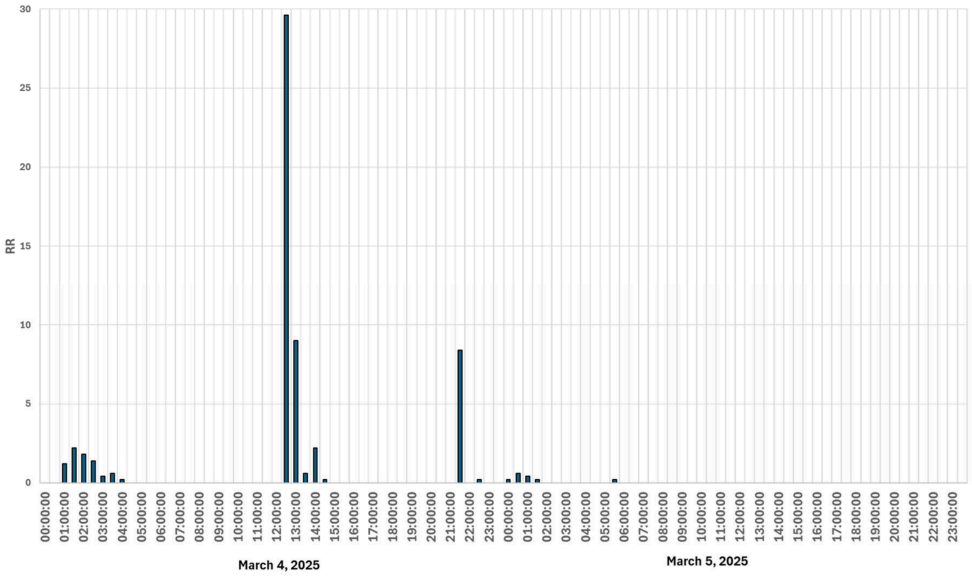


Figure 4. Hourly rainfall intensity Balaraja ARR on 4–5 March 2025.

Long-term rainfall data from the BMKG Budiarto Meteorological Station as shown in Figure 5 were used for frequency and rainfall-shift analysis.

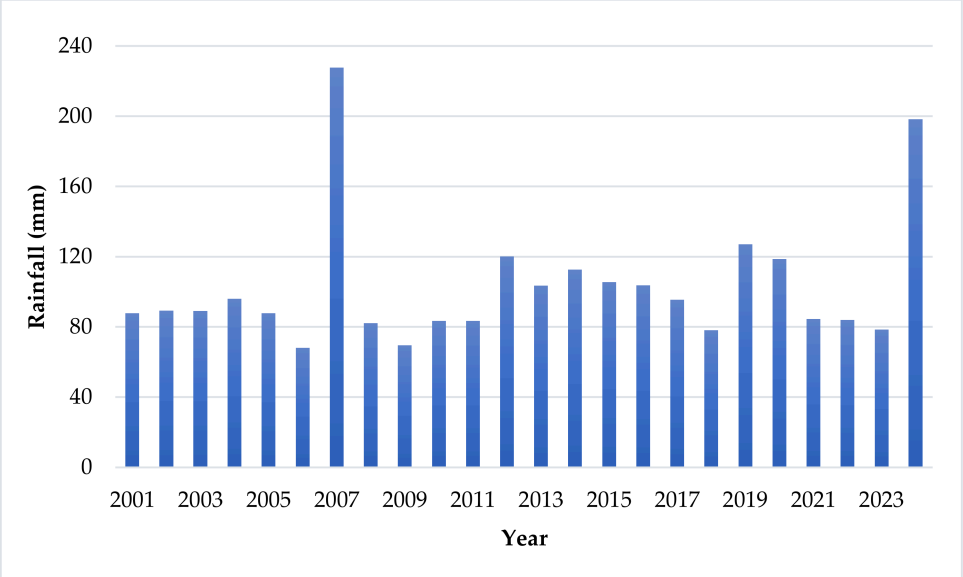


Figure 5. Annual maximum daily rainfall at Budiarto Station.

To examine changes over time, the records were divided into four periods (2001–2013, 2001–2017, 2001–2021, and 2001–2025). Frequency analysis was performed using Hydrognomon to estimate design rainfall under different rainfall shift for selected return periods, and these values were then transformed into design discharge using the calibrated rainfall–runoff model. As a result, the study generated two discharge types: event-based flow from the March 2025 storm and return-period flow under different rainfall-shift scenarios, allowing comparison between observed event response and longer-term rainfall variability.

2.3.2. Spatial Data

Topographical information was derived from a Digital Elevation Model (DEM) provided by the Public Works and Water Resources Agency of Tangerang Regency (Figure 6). The DEM served as the primary elevation input in the HEC-RAS 2D model to define surface flow directions, channel morphology, and floodplain characteristics.

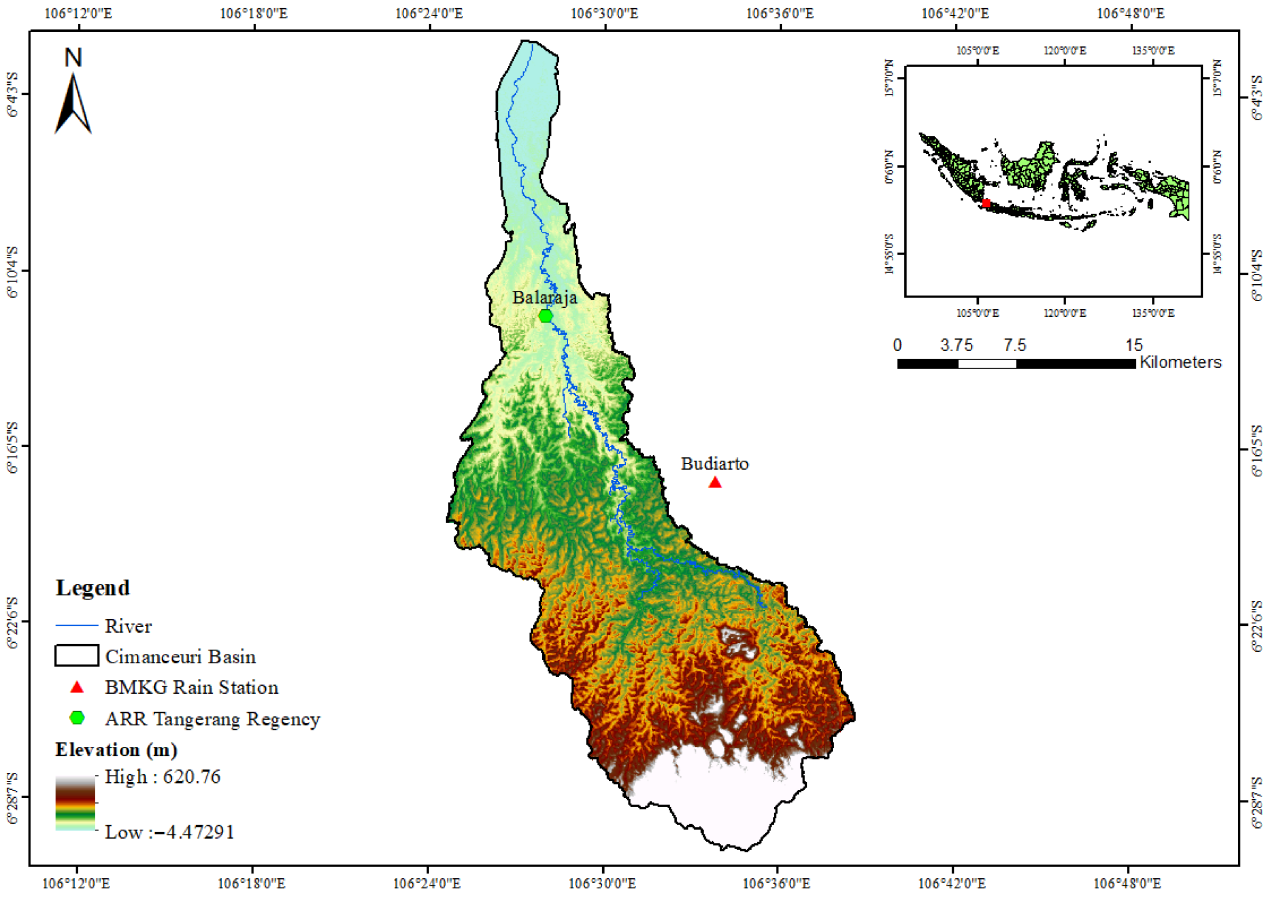


Figure 6. Elevation of Cimanceuri River Basin. The green highlighted area in the inset map indicates Indonesia, while the red dot in the inset map indicates the study location.

2.3.3. Land Use

Tangerang Regency is characterized by a relatively high population density compared to its limited territorial area. Continuous urban development and physical expansion have placed significant pressure on available land resources, particularly vegetated and agricultural areas. The persistent conversion of open land into residential and industrial zones has gradually reduced green space and ecological capacity within the region. Rapid population growth in Tangerang Regency has intensified land use competition, where the increasing demand for housing is not balanced by the availability of suitable residential land [36]. This condition has led to unplanned land conversion, spatial congestion, and the

degradation of environmental quality. Limited land availability in densely populated areas accelerates the decline of vegetated land, contributing to reduced environmental resilience and higher susceptibility to flooding and heat stress [37].

LULC data were obtained from Landsat 7 satellite imagery spanning several time periods between 2013 and 2025. The satellite imagery was classified and validated using visual interpretation to identify changes in built-up areas, vegetation cover, and water bodies. This data was then used to determine CN values and assess the impact of urbanization on surface runoff characteristics across various temporal scenarios.

Land use transformations in the Cimanceuri Watershed in 2013, 2017, 2021, and 2025 can be seen in Figure 7 and the land use conversion matrix in Table 1. Over the 12-year period, significant transformations in land cover patterns were observed, primarily driven by rapid urban development.

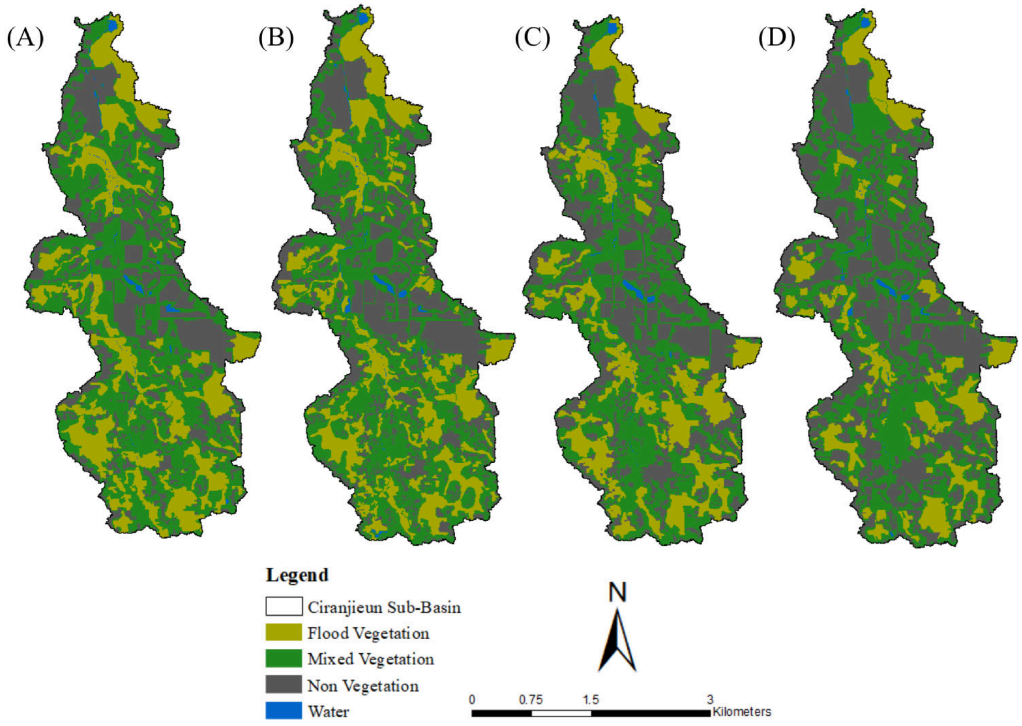


Figure 7. Land use transformation in the Cimanceuri Watershed (**A**) 2013; (**B**) 2017; (**C**) 2021; (**D**) 2025.

Table 1. Areas of different land use patterns in Cimanceuri Watershed from 2013 to 2025 (Ha).

Land Use	Year			
	2013	**2017**	**2021**	**2025**
Non-Vegetation	438.35	512.44	576.74	732.54
Mix-Vegetation	786.48	736.61	686.33	656.39
Flood-Vegetation	433.78	407.86	395.48	283.69
Water	11.88	13.59	11.95	11.46

Table 1 and Figure 7 illustrate the spatial temporal dynamics of land use within the Cimanceuri Watershed between 2013 and 2025. The results clearly indicate a substantial transformation driven by urbanization and land development. The non vegetation (built-up) area increased dramatically from 438.35 Ha in 2013 to 732.54 Ha in 2025, representing a 67% increase over the 12 years period. This expansion primarily occurred in the central and lower sub watershed regions, where residential and industrial growth has been most rapid.

Conversely, both mixed vegetation and floodplain vegetation experienced consistent declines. The mixed vegetation area decreased from 786.48 Ha in 2013 to 634.97 Ha in 2025, while floodplain vegetation dropped from 433.78 Ha to 291.53 Ha, indicating a gradual loss of pervious and high infiltration zones. The water surface area remained relatively constant, fluctuating slightly between 11 and 14 ha, suggesting minimal alteration of open water features.

These trends point to a clear shift from vegetated to impervious surfaces, consistent with intensified urbanization within Tangerang Regency. The conversion of green and floodplain areas into built up land has reduced natural infiltration capacity and surface storage potential, thereby accelerated runoff generation and increased the likelihood of higher peak discharges during rainfall events. Overall, these changes highlight a clear trend of urbanization and vegetation loss, with built-up land replacing natural and agricultural cover types. Such transitions are expected to significantly affect the hydrological characteristics of the sub-basin, particularly by reducing infiltration and increasing surface runoff potential.

2.4. CN Parameterization

SCS-CN method was applied to estimate rainfall–runoff transformation based on land-use and soil characteristics. The CN reflects the runoff potential of a watershed, where higher values indicate lower infiltration and higher surface runoff. This method is widely used in hydrological modelling, particularly in data-scarce regions, due to its simplicity and adaptability. The Curve Number (CN) values assigned to each land-cover class and hydrologic soil group used in this study are presented in Table 2 from USDA [41].

Table 2. SCS Curve Number (CN) values for different land cover types and hydrologic soil groups (USDA, 1984) [41].

Land Cover	HSG A	HSG B	HSG C	HSG D	Description	Source/Table
Water (Open)	100	100	100	100	Water bodies (lakes, rivers, ponds, etc.)	NEH Part 630, Ch. 9, Table 9-1 (Open water)
Trees (Woods, Good)	30	55	70	77	Forested areas with good canopy cover.	TR-55, Table 2-2 (Woods, good condition)
Crops (Rice field)	91	91	91	91	Croplands, especially paddy rice fields.	NEH Part 630, Table A-2 (Rice, flooded)
Built Area	57–85	72	81	86	Human made structures; major road and rail networks; large homogenous impervious surfaces including parking structures, office buildings and residential housing	TR-55 Table 2-2a (1/4 acre lots)
Bare Ground (Unpaved, poor cover)	77	86	91	94	Areas of rock or soil with very sparse to no vegetation for the entire year	NEH Part 630, Ch. 9, Table 9-1 (Fallow, poor condition)
Rangeland (Fair)	49	69	79	84	Open areas covered in homogenous grasses with little to no taller vegetation; wild cereals and grasses with no obvious human plotting	TR-55, Table 2-2 (Pasture, fair condition)

Due to limited discharge data, the simulated HEC-HMS hydrograph was used for hydraulic modelling, with calibration based on inundation extent and water depth. The hydrograph was generated from HEC-HMS was used as input for hydraulic modelling, and calibration was conducted using flood inundation extent and water depth comparison. This approach uses watershed physical characteristics, such as land cover and soil type, to define CN values that represent runoff potential. These CN values are then applied to rainfall data to estimate direct runoff.

The application of the SCS-CN method in the Cimanceuri sub-basin reflects the impact of land-use transformation on watershed hydrological response, as indicated by the increasing CN values. The CN, ranging from 35 to 100, represents the influence of land cover and soil hydrologic group (HSG) on infiltration and runoff, where lower CN values indicate higher infiltration capacity. Land-cover data were obtained from spatial analysis, while soil information was derived from the Harmonized World Soil Database (HWSD) by FAO–IIASA, which classifies soils into HSGs (A–D) based on infiltration potential.

In this study area, the dominant soil type is classified as Hydrologic Soil Group D. The soil classification was derived from the Harmonized World Soil Database (HWSD) and further interpreted using the USDA soil texture triangle to determine the corresponding hydrologic soil group (HSG). The spatial distribution of soil types within the study area is presented in Figure 8.

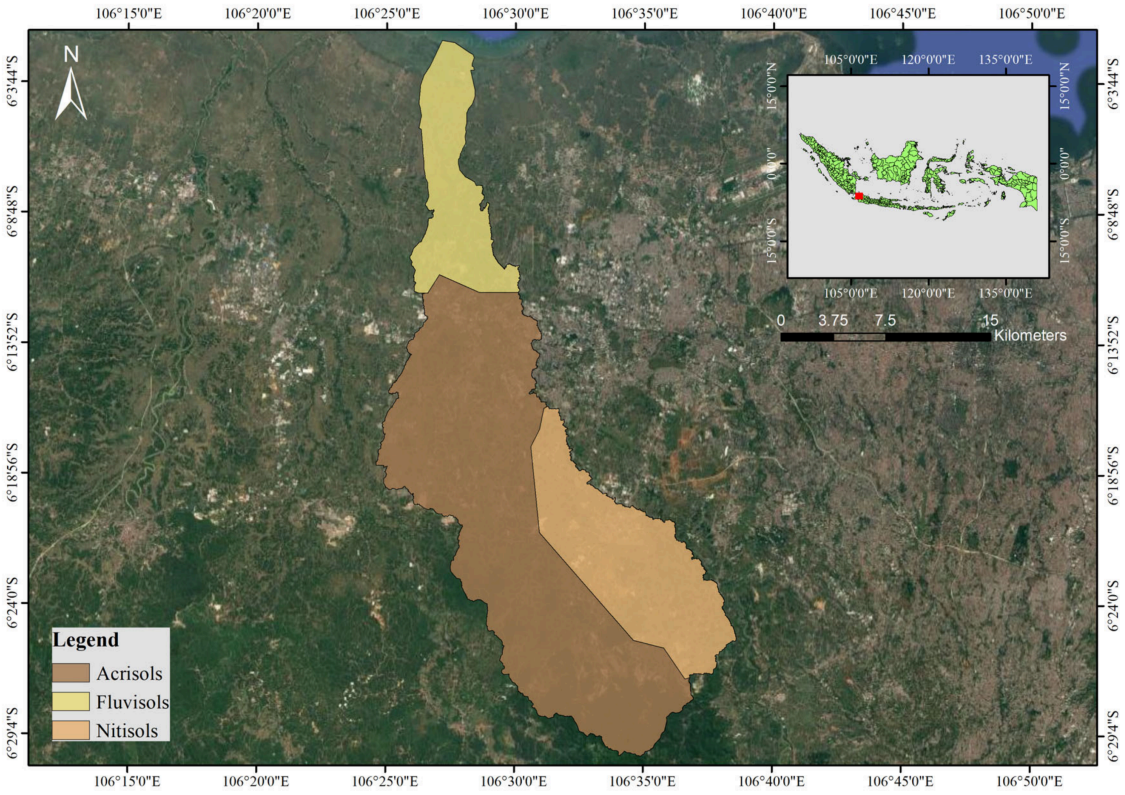


Figure 8. Spatial distribution of soil types in The Cimanceuri sub-basin.

2.5. Framework for Hydrology Analysis

The hydrological analysis in this study was conducted to evaluate the rainfall–runoff response and flood discharge characteristics within the Cimanceuri sub-basin. The analysis comprised two main stages.

First, the flood discharge for the observed event on 4–5 March 2025 was calculated using rainfall data from the Balaraja Automatic Rainfall Recorder. This particular flood event was selected due to its high rainfall intensity and reported inundation within several

downstream areas of the Cimanceuri River, making it representative of current flood conditions in the watershed. The observed data were processed to estimate the peak discharge and to validate the rainfall runoff model performance for the sub-basin (Figure 3).

The design rainfall used in this study was derived from long-term records at the Budiarto Meteorological Station and analyzed under four progressive data windows: 2001–2013, 2001–2017, 2001–2021, and 2001–2025. This approach was applied to capture potential rainfall shifts over time and to assess their influence on hydrological response. Frequency analysis was conducted using Hydrognomon to estimate rainfall depths for selected return periods under each data window. The resulting design rainfall was then associated with corresponding land-use conditions representing 2013, 2017, 2021, and 2025, based on spatial classification results.

Furthermore, the discharge hydrographs obtained from the hydrological modelling were subsequently used as input parameters for hydraulic modelling to generate flood inundation maps. This transition from discharge-based analysis to spatial inundation mapping enables a more comprehensive assessment of flood hazards, as it translates numerical discharge values into spatial representations of flood extent, depth, and distribution. By converting discharge outputs into inundation maps, the study provides a clearer visualization of how land-use changes influence not only the magnitude of runoff but also the spatial expansion of flood-prone areas within the Cimanceuri sub-basin. Consequently, the comparison among different land-use periods (2013, 2017, 2021, and 2025) highlights the progressive impact of surface alteration on flood inundation patterns and associated flood risk.

Design storm hyetographs for each return period were prepared and applied to HEC-HMS model to obtain discharge hydrographs. In addition, the observed rainfall on 5 March 2025 was used to simulate the event hydrograph for calibration. The resulting discharge hydrographs were then used as input in HEC-RAS to assess how land-use changes and variations in rainfall influence flood characteristics in the Cimanceuri River system.

3. Results and Discussion

3.1. Event-Based Hydrological Analysis

Event-based hydrological analysis was conducted using HEC-HMS to simulate the rainfall–runoff response of the Cimanceuri sub-watershed. Based on DEM processing, the model generated key subbasin parameters such as longest flow path, centroidal flow path, channel slope, and basin slope. The CN values were derived separately from land use and soil data using the SCS-CN method (Table 3). These parameters control runoff concentration and hydrograph characteristics and were used in subsequent calibration and simulation steps.

Table 3. Hydrological Characteristics of Cimanceuri Watershed. The highlighted row indicates Subbasin 8, which represents the detailed study area analyzed in this study.

Subbasin	Area (km^2)	Longest Flowpath (km)	L Centroid	L Centroid Slope	Slope Longest Flowpath	Basin Slope	CN (2025)
Subbasin 1	90.1	29.45	13.05	0.002	0.019	0.167	83.84
Subbasin 2	27.89	15.25	7.91	0.002	0.008	0.082	86.26
Subbasin 3	4.16	4.52	2.11	0.003	0.005	0.066	86.95
Subbasin 4	102.43	34.23	20.67	0.001	0.015	0.142	81.5
Subbasin 5	3.46	5.96	2.64	0.002	0.005	0.063	87.75
Subbasin 6	12.31	9.87	3.76	0.001	0.003	0.081	88.76

Table 3. *Cont.*

Subbasin	Area (km^2)	Longest Flowpath (km)	L Centroid	L Centroid Slope	Slope Longest Flowpath	Basin Slope	CN (2025)
Subbasin 7	20.52	19.33	8.81	0.001	0.002	0.076	88.21
Subbasin 8 (Ciranjeun)	16.71	12.54	7.22	0.002	0.003	0.07	86.63
Subbasin 9	1.1	6.3	2.92	0.001	0.002	0.104	89.64
Subbasin 10	99.62	37.19	19.01	0.001	0.002	0.075	86.77
Subbasin 11	4.36	6.54	1.98	0.001	0.004	0.071	86.63
Subbasin 12	35.16	14.93	8.57	0.001	0.002	0.067	86.8
Subbasin 13	22.09	17.24	8.98	0	0.001	0.063	88.92
Subbasin 14	16.66	14.79	7	0.001	0.002	0.054	87.63
Subbasin 15	33.8	15.04	10.16	0	0.001	0.054	92.12

Figure 9 shows the rainfall depth recorded at 30 min intervals during the storm event. The highest rainfall occurred around 12:30 p.m., followed by lower rainfall amounts in the afternoon and a smaller peak around 21:30 p.m. This rainfall pattern was used as input for the HEC-HMS event-based simulation.

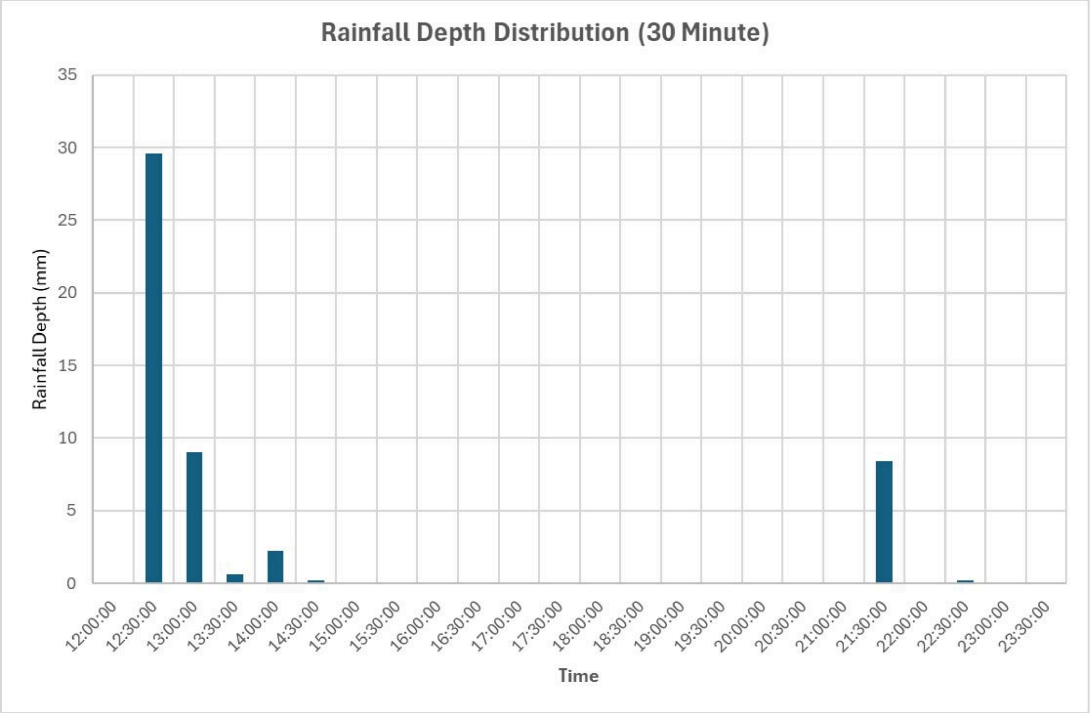


Figure 9. Event-based rainfall depth distribution at 30-min intervals used as input for hydrological modeling distribution.

The simulated flood hydrograph was generated using HEC-HMS based on observed rainfall data that were temporally disaggregated using GPM satellite data. The resulting peak discharge of approximately 37.1 m^3/s was used as the upstream boundary condition in the hydraulic model. Due to the limited availability of observed discharge data, direct validation of the simulated hydrograph was not performed. Instead, calibration was primarily conducted at the hydraulic level through comparison of flood inundation extent and water depth. This limitation is acknowledged, and future work will incorporate observed discharge measurements for more comprehensive validation.

The rainfall–runoff transformation in HEC-HMS applied the SCS-CN method to represent infiltration and surface runoff processes within the subbasin 8. The model generated

an initial abstraction (Ia) value of 7.84 mm and a CN of 86.88, indicating relatively high runoff potential consistent with urban-influenced land-use conditions. These parameters control the proportion of rainfall converted into direct runoff and significantly influence the resulting hydrograph used in subsequent hydraulic simulations.

As shown in the hydrograph of 4–5 March 2025 (Figure 10), the flood discharge exhibits two distinct peaks within the same event. The first and highest peak occurs in the early afternoon, reaching 32.7 m^3/s, indicating a rapid catchment response to intense rainfall. The rising limb is steep, followed by a relatively quick recession, suggesting limited storage capacity and efficient surface runoff conveyance.

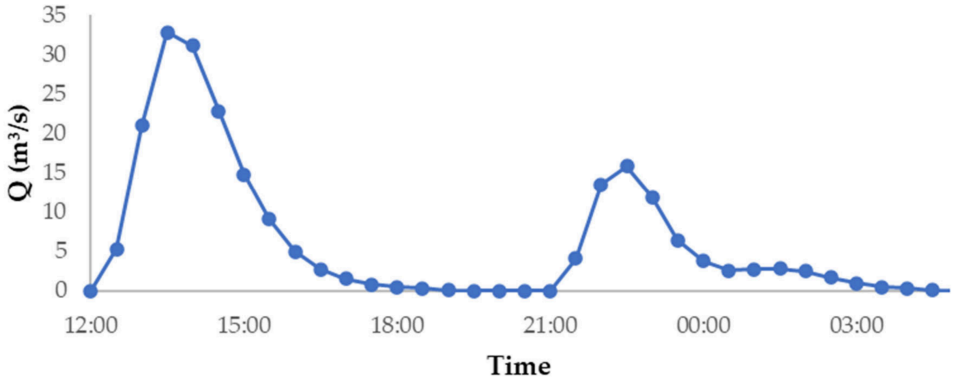


Figure 10. Hydrograph flood discharge on 4–5 March 2025.

After discharge declines to near-baseflow conditions in the evening, a second, smaller peak of about 15.7 m^3/s occurs. This secondary rise likely reflects additional rainfall input or delayed runoff contribution from upstream areas. Following the second peak, the hydrograph gradually recedes toward low flow conditions in the early morning hours. The overall pattern highlights the flashy hydrological behavior of the subbasin during the March 2025 flood event.

The resulting discharge hydrograph was subsequently used as the upstream boundary condition in the HEC-RAS hydraulic model to simulate flow dynamics and flood inundation under various land-use and hydrological scenarios.

3.2. Hydraulic Simulation and Calibration (Event-Based)

Based on the simulation results for the flood event on 5 March 2025, the results are shown in Figures 11 and 12 and Table 4. The simulated inundation height at Al Ikhlas Mosque was 0.43 m, while the height in the imagery was 0.40 m. At Mustika Lake, the simulated inundation height was 0.28 m, and in the imagery, it was 0.2 m. The inundation height at An-Nur Mosque was 0.37 m (simulated) and 0.40 m (photography).

Table 4. Comparison of Observation Data and Modelling Results.

Calibration Point	Flood Height Observation (O) (m)	Flood HeightModel (M) (m)	Difference (O−M)	$(O-M)^2$	$(O-\bar{O})^2$
Al Ikhlas Mosque	0.400	0.430	0.030	0.0009	0.00444
Mustika Lake	0.200	0.280	0.080	0.0064	0.01778
An-Nur Mosque	0.400	0.370	0.030	0.0009	0.00444
Total				0.0082	0.02667
Mean	0.333			0.0027	
RMSE				0.052	
NSE					0.693

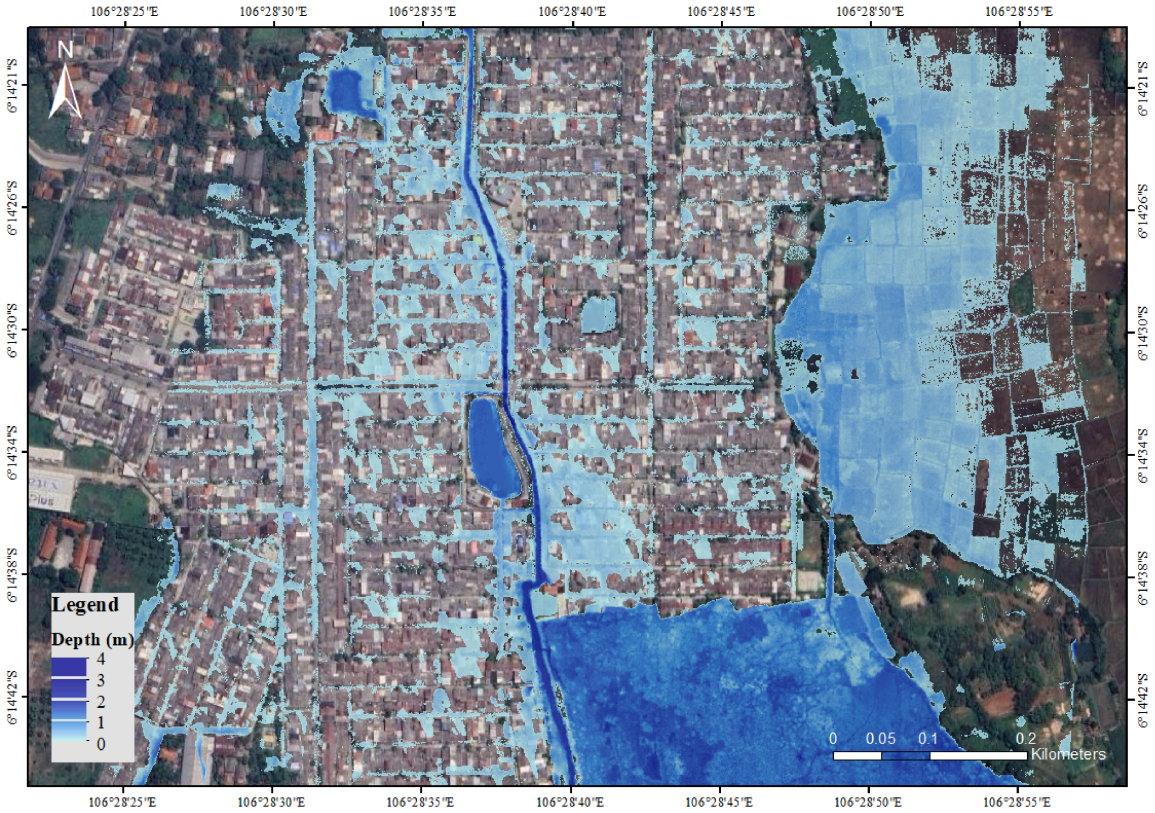


Figure 11. Mustika's residential flood map.

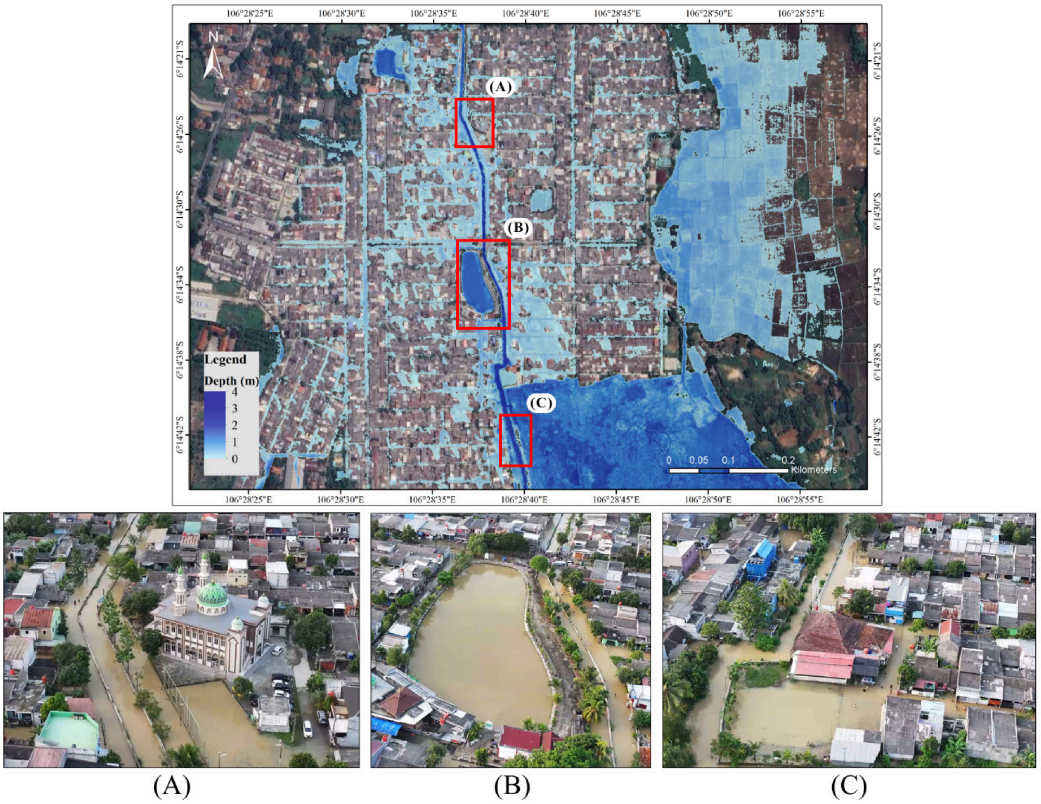


Figure 12. Flood event calibration point.

Specifically, Root Mean Square Error (RMSE) were used to assess the goodness-of-fit between simulated and observed flood depth. The Root Mean Square Error (RMSE) value of

0.052 m indicates a relatively good agreement between observed and simulated flood depths. This indicates that the model shows acceptable agreement with the available observations.

Furthermore, the Nash–Sutcliffe Efficiency (NSE) was calculated to complement the RMSE evaluation, yielding a value of 0.693, which indicates good model performance and indicate that the model can reasonably reproduce the observed flood depths.

Due to data availability constraints, calibration was conducted using the same observed flood event (5 March 2025). While this approach is commonly adopted in data-scarce regions, it introduces limitations in fully assessing model generalizability across different hydrological conditions. Therefore, the model evaluation focused on spatial agreement between simulated and observed inundation patterns, supplemented by statistical performance indicators.

3.3. Simulation Scenario

After completing the calibration process, a series of simulation scenarios were performed to assess flood inundation under various land-use conditions. The comprehensive modelling workflow including model configuration and parameter assignment—is presented in Section 2.2.

The event-based simulations illustrate the watershed's response to the March 2025 storm under different land-use settings; however, they represent only a single event. To obtain a broader understanding of overall flood risk, it is necessary to also examine rainfall associated with different return periods. Therefore, a rainfall-shift analysis was conducted to update the return-period rainfall values and to produce the corresponding design discharge scenarios using extended rainfall records.

The return-period rainfall scenarios were generated from the rainfall-shift analysis of long-term BMKG rainfall data, as detailed in Section 2.2. The resulting design storms were transformed into return-period discharge hydrographs (Qdesign) using the calibrated HEC-HMS model, incorporating land-use conditions and CN values for each year as shown in Table 5.

Table 5. Land Use Distribution and CN for the Cimanceuri Sub-Basin (2013–2025).

Year	Land Use	Area (Ha)	CN	CN × Area	CN
2013	Non-Vegetation	438.35	90.00	39,451.49	85.86
	Mix-Vegetation	786.48	80.50	63,312.02	
	Flood Vegetation	433.78	91.00	39,473.98	
	Water	11.88	100.00	1188.43	
2017	Non-Vegetation	512.44	90.00	46,119.87	86.14
	Mix-Vegetation	736.61	80.50	59,297.10	
	Flood Vegetation	407.86	91.00	37,114.97	
	Water	13.59	100.00	1358.92	
2021	Non-Vegetation	576.74	90.00	51,906.30	86.41
	Mix-Vegetation	686.33	80.50	55,249.37	
	Flood Vegetation	395.48	91.00	35,988.99	
	Water	11.95	100.00	1195.14	
2025	Non-Vegetation	732.54	90.00	65,928.43	86.63
	Mix-Vegetation	634.97	80.50	51,114.69	
	Flood Vegetation	291.53	91.00	26,529.53	
	Water	11.46	100.00	1146.25	

The CN value derived from the SCS-CN method plays a role in determining the proportion of rainfall to runoff. Higher CN values typically occur on impermeable surfaces,

resulting in higher peak discharge and shorter response times. Meanwhile, lower CN values in vegetated areas result in reduced runoff and delayed peaks.

Design rainfall values were estimated using rainfall-shift analysis with progressively extended data windows to reflect temporal changes in rainfall characteristics. The resulting return-period rainfall for the Cimanceuri Watershed under each rainfall-shift period is presented in Table 6. This pattern reflects the impact of expanding impervious surfaces, which reduces infiltration capacity and increases surface runoff. This finding is consistent with fundamental hydrological theory, where increased imperviousness leads to higher runoff coefficients and peak discharge. Similar trends have been widely reported in urbanizing watersheds, highlighting the significant role of land-use change in altering hydrological response and increasing flood risk.

Table 6. Cimanceuri Watershed Design Rainfall under Different Rainfall-Shift Periods.

Return Period (Year)	Design Rainfall (mm)			
	2001–2013	2001–2017	2001–2021	2001–2025
2	85.01	88.18	92.76	90.95
5	105.22	111.06	113.14	115.05
10	127.34	131.50	133.01	138.24
25	171.87	167.70	166.31	179.56

Figure 13 illustrates the relationship between the average CN and the resulting design discharge (Qd) for the 2013–2025 land-use scenarios. The analysis is presented for the 2-year return period, as it represents frequent flood conditions that are more relevant to observed urban flooding in the study area. The graph shows a consistent upward trend, where increasing CN values correspond to higher peak discharge. As the CN rises from 85.86 in 2013 to 86.63 in 2025, the design discharge increases from 73.8 m^3/s to 84.4 m^3/s. This pattern reflects the impact of expanding non-vegetated or impervious areas, which reduce infiltration capacity and increase surface runoff. The correlation analysis suggests that even relatively small increases in CN can lead to noticeable growth in peak discharge, highlighting the hydrological sensitivity of the Cimanceuri sub-basin to land-use change.

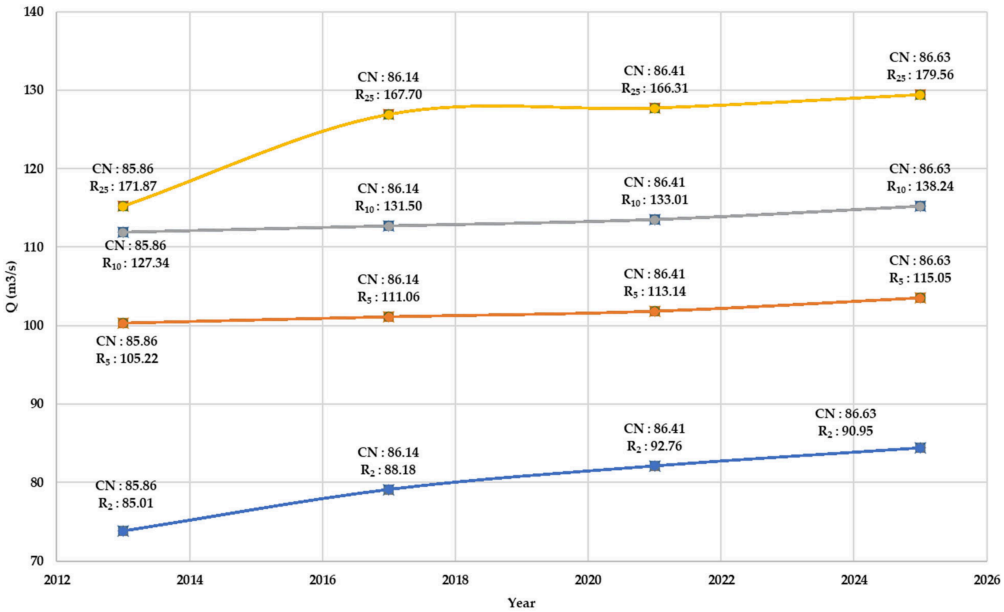


Figure 13. CN vs. discharge graph (2013–2025).

The relationship between increasing CN values and higher peak discharge observed in this study is consistent with findings reported in Indonesian watersheds. Suripin (2004) explained that increases in impervious land cover lead to higher runoff coefficients and more rapid hydrological response, even when changes in CN values are relatively small [42]. Compared to these findings, the trend observed in the Cimanceuri sub-basin indicate that land-use change plays a significant role in amplifying flood discharge, indicating that the watershed is becoming increasingly sensitive to surface runoff generation.

3.4. Two-Dimensional Hydraulic Simulations Under Rainfall-Shift Scenarios and Land Use Change

Following model calibration, 2D hydraulic simulations were performed under rainfall-shift scenarios combined with land-use conditions for 2013, 2017, 2021, and 2025. The return-period discharge hydrographs derived from the rainfall-shift analysis were applied as boundary conditions in the HEC-RAS 2D model, while each simulation incorporated the corresponding land-use map to represent surface changes over time.

This analysis aims to evaluate differences in flood extent and spatial distribution within the same sub-watershed across different periods. By comparing the inundation maps for each scenario, variations in flood patterns and affected areas can be identified, reflecting the combined influence of urbanization and shifting rainfall characteristics on flood behaviour in the Cimanceuri watershed (Figure 14) and (Table 7).

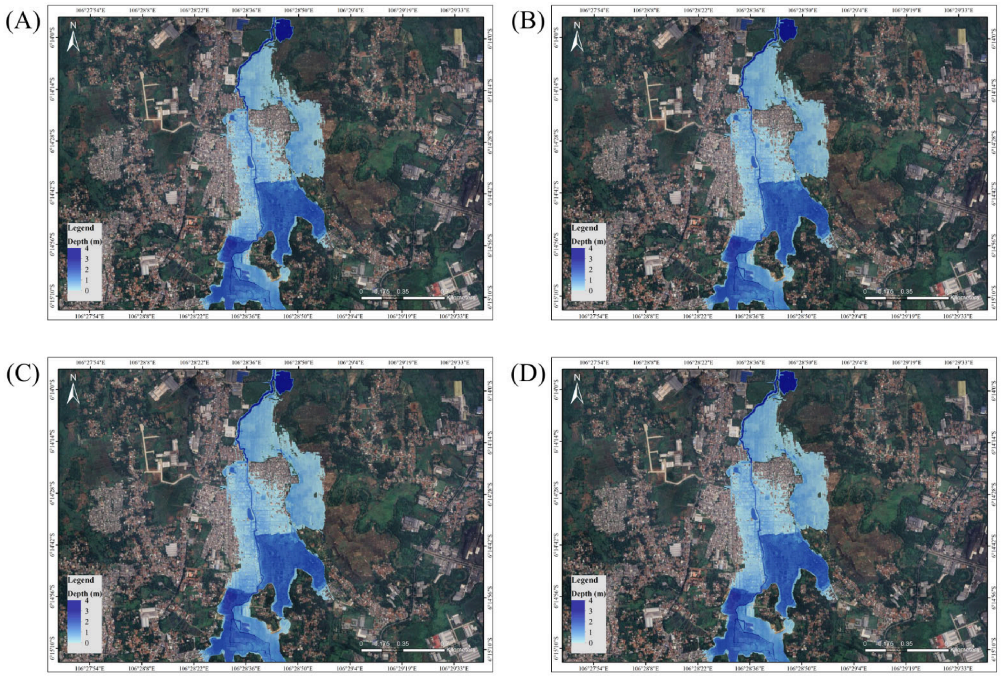


Figure 14. Flood map for 2-year return period: (**A**) 2013, (**B**) 2017, (**C**) 2021, and (**D**) 2025.

Table 7. Flooded Area.

Year	Flooded Area (Ha)
2013	129.91
2017	133.24
2021	136.81
2025	136.10

The results summarized in Table 7 show a gradual increase in total flooded area from 129.91 ha in 2013 to 136.81 ha in 2021, followed by a slight decrease to 136.10 ha in 2025.

Although the change between 2021 and 2025 is relatively small, the overall trend indicates an expansion of inundated area over time compared to the 2013 baseline. This pattern suggests that the combined effects of land-use change and rainfall-shift scenarios have contributed to a measurable increase in flood exposure within the Cimanceuri watershed, particularly during the period of rapid urban development.

The increasing trend in flooded area observed in this study is consistent with findings from flood modelling studies in Indonesia. Kodoatie (2013) highlighted that urban expansion and land-use conversion significantly contribute to the enlargement of flood-prone areas due to reduced infiltration and increased surface runoff [43]. Compared to these findings, the results in the Cimanceuri watershed show a similar pattern of floodplain expansion over time, indicating that land-use change combined with rainfall variability plays a key role in intensifying flood extent, even when the magnitude of change appears relatively moderate.

4. Conclusions

Through an integrated multi-temporal land use analysis (2013–2025) and 2D hydrodynamic modelling (HEC-HMS and HEC-RAS), this study uncovers the complex dynamics between urbanization, rainfall patterns, and flood risk in a tropical region. The findings indicate a significant 67% increase in impervious surface area due to the expansion of residential and industrial sectors. This phenomenon, caused by the shrinking of land vegetation, has overwhelmed natural infiltration functions. The increase in the CN value from 85.86 to 86.63 indicates an increased vulnerability of the region to high surface runoff.

Hydrological simulation results using HEC-HMS show a significant upward trend in peak discharge across all temporal scenarios, with conditions in 2025 recording the highest runoff volume and shortest peak duration. This phenomenon demonstrates the high sensitivity of the catchment area to moderate-intensity rainfall due to the degradation of infiltration capacity. Spatially, the 2D HEC-RAS hydrodynamic modelling recorded a 5.2% expansion of the accumulated area, from 129.9 ha in 2013 to 136.1 ha in 2025. The heaviest impact was experienced by residential areas resulting from the conversion of lowland agricultural land. The validity of this model was shown acceptable agreement with flood observation data (March 2025), with an average deviation below 10%.

This non-linear escalation in flood risk is driven by the synergy between rainfall variability and the extent of impermeable surfaces. These findings underscore the urgency of integrating hydrological risk analysis into development permitting regulations and spatial planning. As a mitigation measure, local governments need to adopt green infrastructure approaches such as infiltration parks, bioretention cells, and constructed wetlands to restore natural watershed retention. Successful flood risk management also requires a cross-sectoral collaborative framework and an integrated data exchange mechanism between hydrometeorological institutions and policymakers to improve the precision of future modelling. However, it should be noted that this analysis is based on a single flood event (5 March 2025), and therefore the transferability of the model to other hydrological conditions remains subject to uncertainty.

Author Contributions: W.A.P.: Conceptualization, Methodology, Original Draft Preparation, Writing, Review and Editing. R.M.F.: Resources, Data Curation, Writing—Review and Editing, Compilation of Feedback. D.Y.: Supervision, Writing—Review and Editing. S.R.R.: Investigation, Analysis. O.T.W.: Investigation, Analysis. All authors have read and agreed to the published version of the manuscript.

Funding: This research received no external funding.

Institutional Review Board Statement: The institutional review board statement is not available.

Informed Consent Statement: The informed consent form is not available.

Data Availability Statement: Data are available on request from the authors.

Acknowledgments: The authors thank Dinas Bina Marga of Tangerang Regency.

Conflicts of Interest: The authors declare no conflicts of interest.

References

1. Li, L.; Yu, Q.; Gao, L.; Yu, B.; Lu, Z. The effect of urban land-use change on runoff water quality: A case study in Hangzhou City. *Int. J. Environ. Res. Public Health* **2021**, *18*, 10748. [CrossRef] [PubMed]
2. Xu, Q.; He, S.; Jiang, J.; Zeng, Z.; Wang, Z.; Duan, H. Assessing the compound impacts of urbanization and climate change on flood hazards in a rapidly urbanized basin. *J. Hydrol. Reg. Stud.* **2025**, *62*, 102942. [CrossRef]
3. Rahman, Z.U.; Zhang, M.; Chen, F.; Ullah, S.; Wang, L.; Ahmad, Z.; Baqa, M.F. Spatiotemporal dynamics of flood susceptibility under future precipitation variability. *Int. J. Appl. Earth Obs. Geoinf.* **2026**, *147*, 105193. [CrossRef]
4. Cui, P.; Peng, J.; Shi, P.; Tang, H.; Ouyang, C.; Zou, Q.; Liu, L.; Li, C.; Lei, Y. Scientific challenges of research on natural hazards and disaster risk. *Geogr. Sustain.* **2021**, *2*, 216–223. [CrossRef]
5. Ernawati, S.K. The concept of disaster and community resilience: A sociological perspective. *Pinisi J. Art Humanit. Soc. Stud.* **2023**, *3*. Available online: https://ojs.unm.ac.id/PJAHSS/article/view/54460 (accessed on 2 January 2026).
6. Nursa'ban, M.; Sugiharyanto, S.; Khotimah, N. Measurement of landslide vulnerability. *J. Penelit. Saintek* **2014**, *15*, 42–58. [CrossRef]
7. Winsemius, H.C.; Aerts, J.C.J.H.; Van Beek, L.P.H.; Bierkens, M.F.P.; Bouwman, A.; Jongman, B.; Kwadijk, J.C.J.; Ligtvoet, W.; Lucas, P.L.; Van Vuuren, D.P.; et al. Global drivers of future river flood risk. *Nat. Clim. Change* **2016**, *6*, 381–385. [CrossRef]
8. Das, S.; Pardeshi, S.D. Comparative analysis of lineaments extracted from DEM data. *Spat. Inf. Res.* **2018**, *26*, 47–57. [CrossRef]
9. Ahmad, D.; Afzal, M. Flood hazards and livelihood vulnerability. *Environ. Sci. Pollut. Res.* **2022**, *29*, 11553–11573. [CrossRef]
10. Dano, U.L.; Alhefnawi, M.A.M.; Al-Shihri, F.; Said, M.A.; Mohamed, E.E.; Alsayed, A.H.A.; Arif, S. Assessing the accuracy of image classification algorithms using TerraSAR-X imagery. *Disaster Adv.* **2020**, *13*, 23–33.
11. Dereli, T.; Eligüzel, N.; Çetinkaya, C. Content analysis using machine learning techniques. *Nat. Hazards* **2021**, *106*, 2025–2045. [CrossRef]
12. Sakurai, M.; Murayama, Y. Information technologies and disaster management. *Prog. Disaster Sci.* **2019**, *2*, 100012. [CrossRef]
13. Yang, Q.; Zheng, X.; Jin, L.; Lei, X.; Shao, B.; Chen, Y. Research progress of urban floods under climate change and urbanization: A Scientometric Analysis. *Buildings* **2021**, *11*, 628. [CrossRef]
14. Wolter, K.; Eischeid, J.K.; Cheng, L.; Hoerling, M. What history tells us about U.S. Rainfall extremes. *Bull. Am. Meteorol. Soc.* **2016**, *97*, S9–S13. [CrossRef]
15. Shuster, W.D.; Bonta, J.; Thurston, H.; Warnemuende, E.; Smith, D.R. Impacts of impervious surface on watershed hydrology. *Urban. Water J.* **2005**, *2*, 263–275. [CrossRef]
16. Li, Y.; Fowler, H.J.; Argüeso, D.; Blenkinsop, S.; Evans, J.P.; Lenderink, G.; Yan, X.; Guerreiro, S.B.; Lewis, E.; Li, X. Strong intensification of hourly rainfall extremes by urbanization. *Geophys. Res. Lett.* **2020**, *47*, e2020GL088758. [CrossRef]
17. Feng, B.; Zhang, Y.; Bourke, R. Urbanization impacts on flood risks. *Nat. Hazards* **2021**, *106*, 613–627. [CrossRef]
18. Tingsanchali, T. Urban flood disaster management. *Procedia Eng.* **2012**, *32*, 25–37. [CrossRef]
19. Yang, L.; Ni, G.; Tian, F.; Niyogi, D. Urbanization exacerbated rainfall under warming climate. *Geophys. Res. Lett.* **2021**, *48*, e2021GL095987. [CrossRef]
20. Westra, S.J.; Fowler, H.J.; Evans, J.P.; Alexander, L.V.; Berg, P.R.; Johnson, F.; Kendon, E.J.; Lenderink, G.; Roberts, N.M. Future changes in extreme rainfall. *Rev. Geophys.* **2014**, *52*, 522–555. [CrossRef]
21. Wang, J.; Hu, C.; Ma, B.; Mu, X. Rapid Urbanization Impact on the Hydrological Processes in Zhengzhou, China. *Water* **2020**, *12*, 1870. [CrossRef]
22. Ramadhan, E.F.; Fidari, J.S.; Harisuseno, D. Flood mapping using HEC-RAS. *J. Teknol. Rekayasa Sumber Daya Air (JTRESDA)* **2024**, *4*, 1205–1218. [CrossRef]
23. Immanuella, L.A.; Dermawan, V.; Winarta, B. Flood control modeling using 2D approach. *J. Tek. Pengair.* **2022**, *13*, 245–257. [CrossRef]
24. Renggono, F.; Lestari, S.; Belgaman, H.A.; Syahdiza, R.; Dewi, S.; Mori, S.; Riawan, E.; Mulyana, E.; Syamsudin, F.; Sulistyowati, R.; et al. Rainfall microphysical characteristics in Jakarta floods. *Sci. Rep.* **2025**, *15*, 33879. [CrossRef] [PubMed]
25. Hermawan, E.; Lubis, S.W.; Harjana, T.; Purwaningsih, A.; Risyanto; Ridho, A.; Andarini, D.F.; Ratri, D.N.; Widyaningsih, R. Large-Scale Meteorological Drivers of the Extreme Precipitation Event and Devastating Floods of Early-February 2021 in Semarang, Central Java, Indonesia. *Atmosphere* **2022**, *13*, 1092. [CrossRef]
26. Rahayu, R.; Mathias, S.A.; Reaney, S.; Vesuviano, G.; Suwarman, R.; Ramdhan, A.M. Impact of land cover, rainfall and topography on flood risk in West Java. *Nat. Hazards* **2023**, *116*, 1735–1758. [CrossRef]

27. Hamdan, A.N.A.; Almuktar, S.; Scholz, M. Rainfall-Runoff Modeling Using the HEC-HMS Model for the Al-Adhaim River Catchment, Northern Iraq. *Hydrology* **2021**, *8*, 58. [CrossRef]
28. El-Bagoury, H.; Gad, A. Integrated Hydrological Modeling for Watershed Analysis, Flood Prediction, and Mitigation Using Meteorological and Morphometric Data, SCS-CN, HEC-HMS/RAS, and QGIS. *Water* **2024**, *16*, 356. [CrossRef]
29. Peker, I.B.; Gülbaz, S.; Demir, V.; Orhan, O.; Beden, N. Integration of HEC-RAS and HEC-HMS with GIS in Flood Modeling and Flood Hazard Mapping. *Sustainability* **2024**, *16*, 1226. [CrossRef]
30. Supratman, M.; Kusuma, S.B.; Cahyono, M.; Kuntoro, A.A. The Impact of Land Use and Land Cover Change Towards Flood Hazard Index in Pondok Karya as Urban Residential Area in Jakarta City, Indonesia. *SSRN* **2024**. [CrossRef]
31. Yang, L.; Smith, J.; Wright, D.; Baeck, M.; Villarini, G.; Tian, F.; Hu, H. Urbanization and climate change impacts on flooding: An examination of nonstationarities in urban flooding. *J. Hydrometeorol.* **2013**, *14*, 1791–1809. [CrossRef]
32. USACE. HEC-HMS Hydrologic Modeling System User Manual. 2025. Available online: https://www.hec.usace.army.mil/software/hec-hmshttps://www.hec.usace.army.mil/software/hec-hms (accessed on 2 January 2026).
33. Hasan, H.H.; Mohd Razali, S.F.; Ahmad Zaki, A.Z.I.; Mohamad Hamzah, F. Integrated Hydrological-Hydraulic Model for Flood Simulation in Tropical Urban Catchment. *Sustainability* **2019**, *11*, 6700. [CrossRef]
34. Zhang, L.; Nan, Z.; Xu, Y.; Li, S. Hydrological Impacts of Land Use Change and Climate Variability in the Headwater Region of the Heihe River Basin, Northwest China. *PLoS ONE* **2016**, *11*, e0158394.
35. Hounkpè, J.; Diekkrüger, B.; Afouda, A.A.; Sintondji, L.O.C. Land use change increases flood hazard: A multi-modelling approach to assess change in flood characteristics driven by socio-economic land use change scenarios. *Nat. Hazards* **2019**, *96*, 571–593. [CrossRef]
36. USACE (U.S. Army Corps of Engineers). *HEC-RAS River Analysis System, User's Manual*; Hydrologic Engineering Center (HEC): Davis, CA, USA. Available online: https://www.hec.usace.army.mil/confluence/display/RASUM (accessed on 2 January 2026).
37. Nurul, M.; Prasiamratri, N.; Elvira, W.; Safitri, W.; Prabowo, R. Kondisi Tutupan Lahan di Kabupaten Tangerang Berdasarkan Indeks Vegetasi. *J. Geosains Remote Sens.* **2021**, *2*, 1–7. [CrossRef]
38. Öztürk, Ş.; Yılmaz, K.; Dinçer, A.E.; Kalpakcı, V. Effect of urbanization on surface runoff and performance of green roofs and permeable pavement for mitigating urban floods. *Nat. Hazards* **2024**, *120*, 12375–12399. [CrossRef]
39. Dang, A.T.N.; Kumar, L. GIS-based flood risk analysis. *Geomat. Nat. Hazards Risk* **2017**, *8*, 1792–1811. [CrossRef]
40. Nash, J.E.; Sutcliffe, J.V. River flow forecasting through conceptual models. *J. Hydrol.* **1970**, *10*, 282–290.
41. USDA Soil Conservation Service. *National Engineering Handbook (NEH), Section 4: Hydrology, Ch. 9*; USDA Soil Conservation Service: Washington, DC, USA, 1984.
42. Suripin. *Sustainable Urban Drainage Systems*; Andi: Yogyakarta, Indonesia, 2004.
43. Kodoatie, R.J. *Urban Flood Engineering and Management*; Andi: Yogyakarta, Indonesia, 2013.

Disclaimer/Publisher's Note: The statements, opinions and data contained in all publications are solely those of the individual author(s) and contributor(s) and not of MDPI and/or the editor(s). MDPI and/or the editor(s) disclaim responsibility for any injury to people or property resulting from any ideas, methods, instructions or products referred to in the content.